

PCCP

Accepted Manuscript



This is an *Accepted Manuscript*, which has been through the Royal Society of Chemistry peer review process and has been accepted for publication.

Accepted Manuscripts are published online shortly after acceptance, before technical editing, formatting and proof reading. Using this free service, authors can make their results available to the community, in citable form, before we publish the edited article. We will replace this *Accepted Manuscript* with the edited and formatted *Advance Article* as soon as it is available.

You can find more information about *Accepted Manuscripts* in the [Information for Authors](#).

Please note that technical editing may introduce minor changes to the text and/or graphics, which may alter content. The journal's standard [Terms & Conditions](#) and the [Ethical guidelines](#) still apply. In no event shall the Royal Society of Chemistry be held responsible for any errors or omissions in this *Accepted Manuscript* or any consequences arising from the use of any information it contains.

Oxygen nonstoichiometry, defect equilibrium model and thermodynamic quantities in the Ruddlesden–Popper oxide $\text{Sr}_3\text{Fe}_2\text{O}_{7-\delta}$

Yihan Ling,^{*a} Fang Wang,^a Riyan Achmad Budiman,^b Takashi Nakamura^a and

Koji Amezawa^a

Oxygen nonstoichiometry of the Ruddlesden–Popper oxide $\text{Sr}_3\text{Fe}_2\text{O}_{7-\delta}$ was measured at intermediate temperatures (773–1073 K) by the coulometric titration and the high temperature gravimetry. The oxygen nonstoichiometric behavior was analyzed by the defect equilibrium model with localized electrons. From the defect chemical analysis, estimated oxygen vacancy concentration at the O3 sites increases and at the O1 sites decreases with the increasing temperatures. This characteristic behavior is considered to be caused by the redistribution of oxygen and vacancy between the O1 and O3 sites. The obtained thermodynamic quantities of partial molar enthalpy of oxygen, $h_{\text{O}} - h_{\text{O}}^{\circ}$, and partial molar entropy of oxygen, $s_{\text{O}} - s_{\text{O}}^{\circ}$, calculated from the Gibbs–Helmholtz equation are in good agreements with ones from the statistical thermodynamic calculation based on the defect equilibrium model, indicating that the proposed defect equilibrium model is reasonable.

www.rsc.org/pccp

1. Introduction

Recently, layered oxide materials with mixed ionic-electronic conductivity and high catalytic activity such as double perovskites and the Ruddlesden–Popper series have been widely investigated because of their potential application in electrochemical devices, such as electrodes in solid oxide fuel cells (SOFCs), oxygen permeation membranes, and methane conversion reactors.^{1–6} In particular, the Ruddlesden–Popper type oxide $\text{Sr}_3\text{Fe}_2\text{O}_{7-\delta}$ belongs to the space group $I4/mmm$ with tetragonal symmetry, consisting of the same element as typical perovskite $\text{SrFeO}_{3-\delta}$.^{7–16} It has three different anion positions: O1 is the oxygen site between two FeO_6 octahedrons along c axis, O2 is the oxygen site at the apex oxygen of FeO_6 adjacent to the rock salt layer, and O3 is the oxygen site between two FeO_6 along ab plane as shown in Fig. 1.

Compared to simple perovskite $\text{SrFeO}_{3-\delta}$, the Ruddlesden–Popper type oxide $\text{Sr}_3\text{Fe}_2\text{O}_{7-\delta}$ seems to improve the structural stability and the oxygen transport property.^{14, 17, 18} It can tolerate a large oxygen nonstoichiometry without structural transformation and possess several different oxygen-ion transport pathways. At low temperatures, oxygen vacancies are preferentially located at the O1 sites with the most likely oxygen-ion transport pathways of $\text{O3} \rightarrow \text{O1} \rightarrow \text{O3}$ jumps along the octahedral edges while oxygen vacancies at the O2 sites can be ignored.^{10, 11} When temperature increases, oxygen vacancy concentration at the O3 sites increases due to vacancy redistribution between the O1 and O3 sites, suggesting that the oxygen-ion diffusion can be accelerated.^{12–14} If the temperature is higher than 1100 K, the directly $\text{O3} \rightarrow \text{O3}$ jumps can happen.^{8, 11, 13–15} In earlier studies with the assumption that oxygen vacancies are distributed with identical probability in the different oxygen positions, the simple defect equilibrium model was evaluated to analysis the oxygen nonstoichiometry of $\text{Sr}_3\text{Fe}_2\text{O}_{7-\delta}$ at high $P(\text{O}_2)$ and high temperatures.^{11, 15} Recently, V.V. Kharton *et al.*¹⁴ reported that Sc-doped $\text{Sr}_3\text{Fe}_2\text{O}_{7-\delta}$ system can increase the vacancy concentration at the O3 sites leading to the increasing ionic conductivity. In addition, Mo-doped $\text{Sr}_3\text{Fe}_2\text{O}_{7-\delta}$ system was explored

to be used under reducing condition and analyzed by a more complex defect equilibrium model with oxygen vacancy redistribution between the O1 and O3 sites.¹⁶ However, the details about oxygen vacancy redistribution between the O1 and O3 sites in $\text{Sr}_3\text{Fe}_2\text{O}_{7-\delta}$ system especially at intermediate temperatures (773–1073 K) and low $P(\text{O}_2)$ are critical but missing for oxygen vacancy formation and the oxygen-ion migration mechanism as well as the potential electrochemical application.^{19–21}

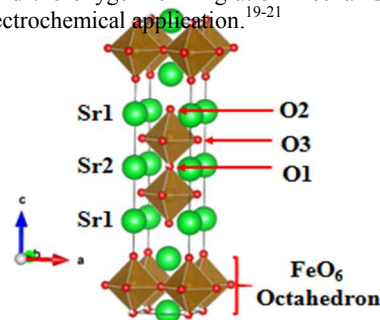


Fig.1 Crystal structure of the Ruddlesden–Popper oxide $\text{Sr}_3\text{Fe}_2\text{O}_{7-\delta}$

The aim of this study is to elucidate how oxygen nonstoichiometric behavior and defect structure emerges and varies in the Ruddlesden–Popper $\text{Sr}_3\text{Fe}_2\text{O}_{7-\delta}$ at intermediate temperatures (773–1073 K). Besides, for the control of material properties and optimized design for practical applications, the variation of the oxygen nonstoichiometry and the defect equilibrium model are very essential. In this work, oxygen nonstoichiometry in $\text{Sr}_3\text{Fe}_2\text{O}_{7-\delta}$ was measured and analyzed based on the defect equilibrium model with localized electrons and the oxygen vacancy redistribution between the O1 and O3 sites. In addition, the statistical thermodynamic calculation was carried out for the oxygen nonstoichiometry data to elucidate the partial molar enthalpy and entropy of oxygen based on the proposed defect equilibrium model.

2. Experimental

2.1 Sample preparation and HT-XRD measurement

The Ruddlesden–Popper oxide $\text{Sr}_3\text{Fe}_2\text{O}_{7-\delta}$ was synthesized via solid-state reaction route. The stoichiometric amounts of high-purity SrCO_3 and Fe_2O_3 (99.99%, RARE METALLIC) were mixed and thoroughly ground with ethanol, and then calcined in air at 1473 K for 10 h with 2–3 intermediate grindings. The phase purity at room temperature were measured by powder X-ray diffraction (D2 Phaser: Cu $K\alpha$ radiation, Bruker AXS, Germany) and the lattice parameters were obtained from the diffraction patterns by the Whole Powder Pattern Decomposition with the TOPAS software.²² The synthesized $\text{Sr}_3\text{Fe}_2\text{O}_{7-\delta}$ was confirmed to be a single phase (Fig. 2(a)) having a tetragonal structure (space group $I4/mmm$) with the unit cell parameters $a = 3.8634257 \text{ \AA}$ and $c = 20.1529667 \text{ \AA}$. The refinement of the $\text{Sr}_3\text{Fe}_2\text{O}_{7-\delta}$ sample gave R_{exp} , wR_p , R_p and GOF values of 3.71%, 4.85%, 3.79% and 1.31, respectively. Since a water-containing derivative of $\text{Sr}_3\text{Fe}_2\text{O}_{7-\delta}$ can be easily formed when subjected to the ambient atmosphere below 587 K.^{23–26} An X-ray diffractometer (D8 Advance with LYNXEYEM Super Speed Detector, Bruker AXS, and Cu- $K\alpha$ radiation) was used to evaluate the phase stability of $\text{Sr}_3\text{Fe}_2\text{O}_{7-\delta}$ at 773–1173 K. Fig. 2 (b) shows the HT-XRD results of $\text{Sr}_3\text{Fe}_2\text{O}_{7-\delta}$ at $P(\text{O}_2)=0.01$ bar and no phase transition was observed during 773–1173 K with the holding time of 5 h, indicating the good stability at relatively high temperatures.

2.2 Oxygen nonstoichiometry measurement

The oxygen nonstoichiometry in the $P(\text{O}_2)$ range of 10^{-4} to 1 bar was measured by the high temperature gravimetry using a microbalance ((Cahn D200, Thermo Fisher Scientific Inc., Waltham, MA, USA)). A cylindrical pellet of about 0.5 g was pressed and heated at 1173 K to form a porous specimen. That was placed into a silica basket suspended by Pt wires from the beam of the microbalance. $P(\text{O}_2)$ was controlled by Ar- O_2 gas mixtures and was monitored by zirconia sensors at the gas inlet, outlet and inside the sample chamber. Equilibrium between the sample and surrounding gas atmosphere was confirmed by the stable sample weight and $P(\text{O}_2)$.

The variation of oxygen nonstoichiometry $\Delta\delta$ can be calculated according to the weight change of the sample, Δw_s , by:

$$\Delta\delta = \frac{M_S \Delta w_S}{M_{\text{O}} w_S} \quad (1)$$

Where M_S , M_{O} , and w_S are the formula weight of the sample and oxygen atom, and the weight of the specimen, respectively. The absolute value of the oxygen content was determined from the weight change of the specimen by the decomposition in H_2 atmosphere.

The coulometric titration was carried out to measure the oxygen nonstoichiometry under the oxygen partial pressure below 10^{-3} bar and the detail structure of the coulometric titration cell was shown in ref.27. About 0.5g of the pressed $\text{Sr}_3\text{Fe}_2\text{O}_{7-\delta}$ sample was slightly sintered (1173 K for 2 h). After the heat treatment, the sample became agglomeration of coarse grains, then the sample was placed into YSZ electrolyte tube and firmly pressed by Pt foil supported by Al_2O_3 tube against the inner wall of YSZ tube. Pt paste was painted on the outside of YSZ tube forming a galvanic cell, where the oxygen partial pressure of the sample $P(\text{O}_{2,\text{II}})$ was obtained from the equilibrium electromotive force E under open circuit conditions according to the Nernst equation:

$$E = \frac{RT}{4F} \ln \left(\frac{P(\text{O}_{2,\text{II}})}{P(\text{O}_{2,\text{I}})} \right) \quad (2)$$

Where R , T , F and $P(\text{O}_{2,\text{I}})$ are the ideal gas constant ($8.31447 \text{ J} \cdot \text{mol}^{-1} \cdot \text{K}^{-1}$), the temperature in Kelvin, Faraday constant and the oxygen partial pressure in air. Prior to sealing, the YSZ tube was evacuated to about 10^{-1} bar by exchanging with argon gas several times to reduce the amount of residual oxygen inside the tube.

Because the sample directly contacts with the YSZ wall as one electrode, $\Delta\delta$ of the sample can be calculated by the electric charge, C , through the cell:

$$\Delta\delta = \frac{MSC}{2wsF} \quad (3)$$

The coulometric titration cell was successfully applied to measure oxygen nonstoichiometry of $\text{La}_{1-x}\text{Sr}_x\text{MnO}_{3-\delta}$, $\text{La}_{0.6}\text{Sr}_{0.4}\text{Co}_{1-y}\text{Fe}_y\text{O}_{3-\delta}$ and $\text{La}_{2-x}\text{Sr}_x\text{NiO}_{4-\delta}$.^{28–30}

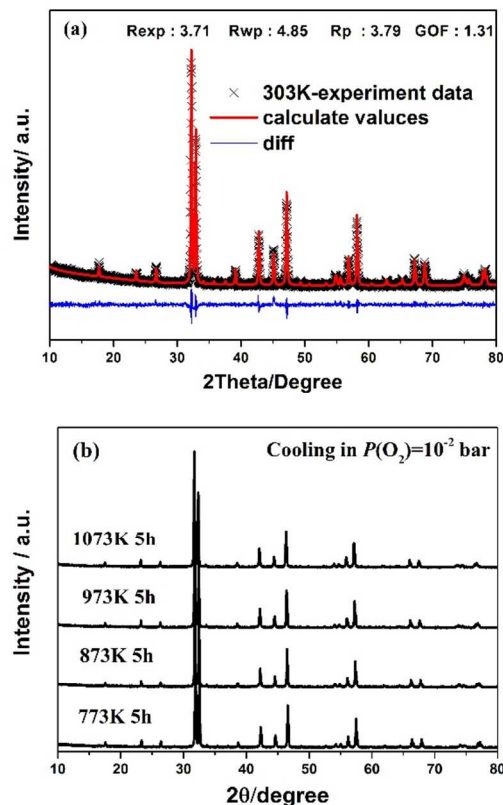
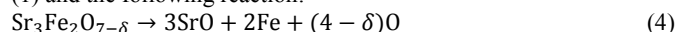


Fig.2 (a) The result of the whole pattern fitting for XRD pattern of $\text{Sr}_3\text{Fe}_2\text{O}_{7-\delta}$ measured at room temperature. $R_{\text{exp}}=3.71\%$, $wR_p=4.85\%$, $R_p=3.79\%$, and $\text{GOF}=1.31$. (b) HT-XRD results of $\text{Sr}_3\text{Fe}_2\text{O}_{7-\delta}$ at $P(\text{O}_2)=0.01$ bar during 773–1173 K with the holding time of 5 h.

3. Results and discussion

3.1 Oxygen nonstoichiometry of $\text{Sr}_3\text{Fe}_2\text{O}_{7-\delta}$

The oxygen nonstoichiometry of $\text{Sr}_3\text{Fe}_2\text{O}_{7-\delta}$ was measured by the high-temperature gravimetry (the weight change depend on $P(\text{O}_2)$) and the coulometric titration (the variation of oxygen content depend on the applied electrical charge). The absolute value of the oxygen content in $\text{Sr}_3\text{Fe}_2\text{O}_{7-\delta}$ was determined by the decomposition of the sample in H_2 atmosphere. First, the high-temperature gravimetry measurements were finished in the temperature range between 773 and 1073 K and the $P(\text{O}_2)$ range between 10^{-4} and 1 bar. Then the sample was heated in 100 ppm bar O_2 -Ar at 1173 K followed by flashing the sample chamber using 1 bar Ar until the sample weight and $P(\text{O}_2)$ were both constant. Finally, the gas was switched to 1 bar H_2 and then a very rapid decline of $P(\text{O}_2)$ was observed within the first few minutes as shown in Fig. 3(a), while the weight of the sample gradually decreased. When the sample weight and $P(\text{O}_2)$ reached stable values, the full decomposition of $\text{Sr}_3\text{Fe}_2\text{O}_{7-\delta}$ was completed and the absolute value of the oxygen content can be calculated from the weight change of the sample according to Eqs. (1) and the following reaction:



Only strontium oxide and iron were observed from the decomposed sample by the XRD measurement as shown in Fig. 3 (b).

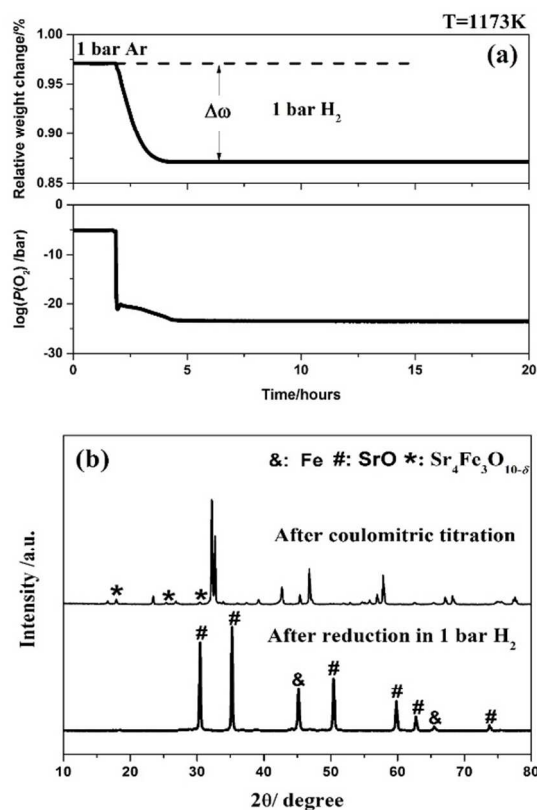


Fig.3 (a) The variation of the sample weight and $P(\text{O}_2)$ with thermogravimetry results of the full decomposition of $\text{Sr}_3\text{Fe}_2\text{O}_{7-\delta}$ at 1173 K. (b) XRD patterns of $\text{Sr}_3\text{Fe}_2\text{O}_{7-\delta}$ at room temperature after reduction in 100% H_2 and after the coulometric titration.

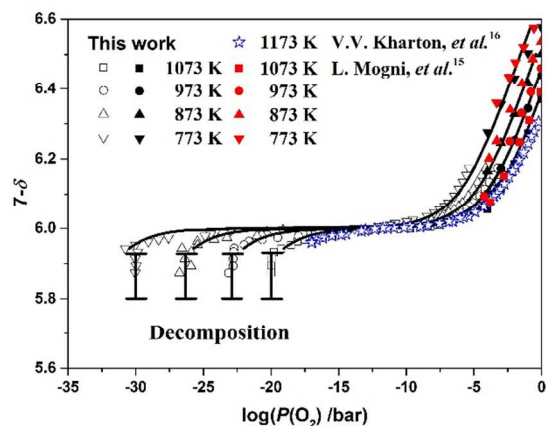


Fig.4 Oxygen nonstoichiometry (shown as $7-\delta$) of $\text{Sr}_3\text{Fe}_2\text{O}_{7-\delta}$ as a function of $P(\text{O}_2)$ at 773–1073 K. Closed and open symbols show the data points measured by the high temperature gravimetry and the coulometric titration, respectively. The solid lines are the calculated results of the defect equilibrium model (Eqs. (24)). Comparison of oxygen nonstoichiometry with data from the literature (L. Mogni *et al.*¹⁵ and V.V. Kharton *et al.*¹⁶).

Fig.4 shows the oxygen nonstoichiometry of $\text{Sr}_3\text{Fe}_2\text{O}_{7-\delta}$ at intermediate temperatures between 773 and 1073 K and the $P(\text{O}_2)$

range between 10^{-30} and 1 bar. Closed and open symbols show the data points measured by the high temperature gravimetry and the coulometric titration, respectively. The results of the high temperature gravimetry and the coulometric titration showed good agreements. At high $P(\text{O}_2)$ range measured by high temperature gravimetry, the oxygen content of the sample gradually decreased with the decreasing $P(\text{O}_2)$ and increasing temperature. Coulometric titration was carried out in intermediate $P(\text{O}_2)$ range instead of the high temperature gravimetry measurement using the $\text{CO}-\text{CO}_2$ mixtures to avoid reactions with the gas phase.³¹⁻³³ The slopes of δ vs $P(\text{O}_2)$ gradually reduced and the $P(\text{O}_2)$ dependencies of the oxygen nonstoichiometry exhibited a typical plateaus at $\delta \sim 1.0$, where the average oxidation state of iron is 3+. With further reduce of $P(\text{O}_2)$, the oxygen content decreased more and the abruptly changes of oxygen content happened at the decomposition $P(\text{O}_2)$, which was given by vertical lines in Fig. 4, indicating that the sample began to decompose and a second phase emerged, as shown in Fig. 3(b). The measured oxygen nonstoichiometry of $\text{Sr}_3\text{Fe}_2\text{O}_{7-\delta}$ is also in good agreements with those reported by L. Mogni *et al.*¹⁵ and V.V. Kharton *et al.*¹⁶ (as shown in Fig.4).

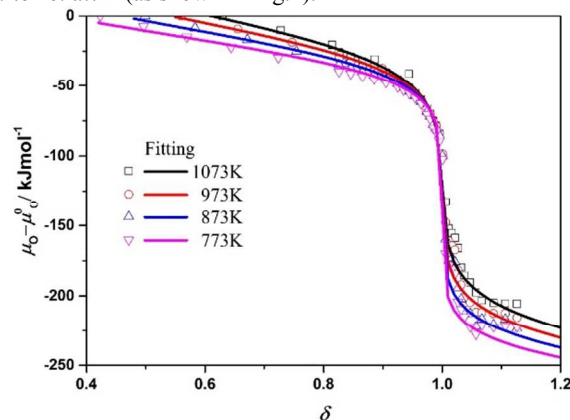


Fig.5 The oxygen chemical potential for $\text{Sr}_3\text{Fe}_2\text{O}_{7-\delta}$. Solid lines are calculated by Eqs. (43).

3.2 The calculation of thermodynamic quantities

The oxygen chemical potential, $\mu_{\text{O}} - \mu_{\text{O}}^{\circ}$, of $\text{Sr}_3\text{Fe}_2\text{O}_{7-\delta}$ in equilibrium with gas at a certain oxygen partial pressure and temperature can be expressed by:

$$\mu_{\text{O}} - \mu_{\text{O}}^{\circ} = \frac{RT}{2} \ln P(\text{O}_2) \quad (5)$$

where μ_{O}° are μ_{O} in equilibrium with 1 bar oxygen. The equilibrium isotherms of the oxygen chemical potential, $\mu_{\text{O}} - \mu_{\text{O}}^{\circ}$, as a function of oxygen nonstoichiometry of $\text{Sr}_3\text{Fe}_2\text{O}_{7-\delta}$ are displayed in Fig. 5. From the Gibbs–Helmholtz equation, the partial molar enthalpy of oxygen, $h_{\text{O}} - h_{\text{O}}^{\circ}$, and partial molar entropy of oxygen, $s_{\text{O}} - s_{\text{O}}^{\circ}$, can be calculated by:

$$h_{\text{O}} - h_{\text{O}}^{\circ} = \frac{\partial}{\partial(1/T)} \left(\frac{RT}{2} \ln P(\text{O}_2) \right) \quad (6)$$

$$s_{\text{O}} - s_{\text{O}}^{\circ} = -\frac{\partial}{\partial T} \left(\frac{RT}{2} \ln P(\text{O}_2) \right) \quad (7)$$

Fig. 6 shows $R/2 \ln P(\text{O}_2)$ vs. $1/T$ plots and $RT \ln P(\text{O}_2)$ vs. T plots of $\text{Sr}_3\text{Fe}_2\text{O}_{7-\delta}$ for the selected δ , respectively, and both curves seem to be almost linear. $h_{\text{O}} - h_{\text{O}}^{\circ}$ and $s_{\text{O}} - s_{\text{O}}^{\circ}$ given in Fig. 7, can be calculated from the slopes of the plots because they are essentially independent of temperature. From the shapes of $\mu_{\text{O}} - \mu_{\text{O}}^{\circ}$, $h_{\text{O}} - h_{\text{O}}^{\circ}$ and $s_{\text{O}} - s_{\text{O}}^{\circ}$ of $\text{Sr}_3\text{Fe}_2\text{O}_{7-\delta}$ around $\delta=1$, the abrupt changes of thermodynamic quantities indicated that the major defect species suddenly changes at the average oxidation state of iron is 3+. The abrupt variations of $\mu_{\text{O}} - \mu_{\text{O}}^{\circ}$, $h_{\text{O}} - h_{\text{O}}^{\circ}$ and $s_{\text{O}} - s_{\text{O}}^{\circ}$ curvature of $\text{Sr}_3\text{Fe}_2\text{O}_{7-\delta}$ as δ approaches 1. The behavior of oxygen nonstoichiometry and thermodynamic quantities of $\text{Sr}_3\text{Fe}_2\text{O}_{7-\delta}$ are

very similar to those of $\text{La}_{1-x}\text{Sr}_x\text{FeO}_{3-\delta}$ analyzed by the defect equilibrium model with an ideal solution approximation.³⁴ Therefore we assume an ideal solution approximation in this study by the comparison those of $\text{La}_{1-x}\text{Sr}_x\text{CoO}_{3-\delta}$,^{29, 34-36} $\text{La}_{1-x}\text{Sr}_x\text{FeO}_{3-\delta}$,³⁴ $\text{La}_{0.6}\text{Sr}_{0.4}\text{Co}_{1-y}\text{Fe}_y\text{O}_{3-\delta}$ and $\text{La}_{2-x}\text{Sr}_x\text{NiO}_{4+\delta}$.

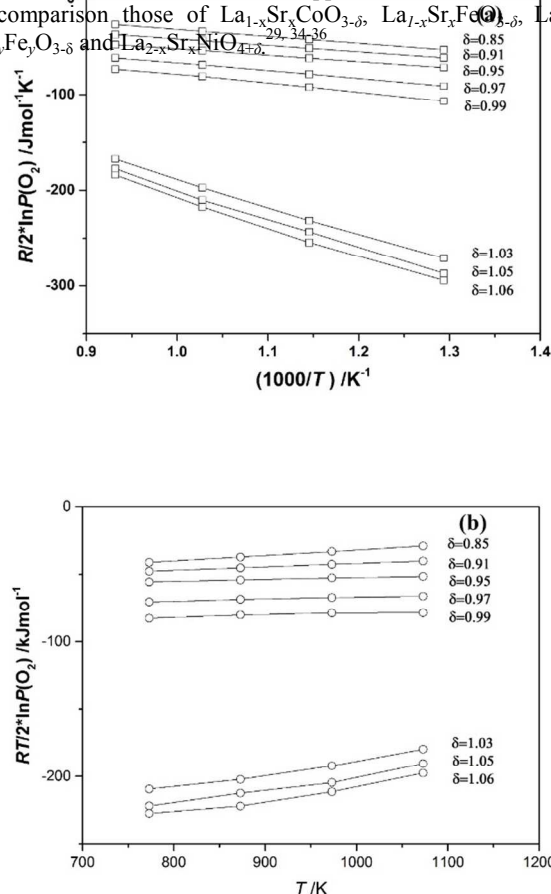
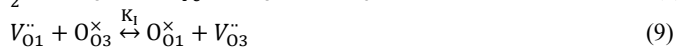
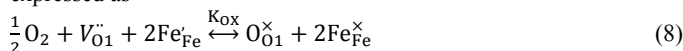


Fig.6 The relationship between $R/2 \ln P(\text{O}_2)$ and $1/T$ (a) and $RT/2 \ln P(\text{O}_2)$ and T (b) of $\text{Sr}_3\text{Fe}_2\text{O}_{7-\delta}$ at selected oxygen nonstoichiometry.

3.3 Defect equilibrium model for $\text{Sr}_3\text{Fe}_2\text{O}_{7-\delta}$

In order to explain the oxygen nonstoichiometric behavior of $\text{Sr}_3\text{Fe}_2\text{O}_{7-\delta}$, the defect equilibrium model with localized electrons is constructed in this study because the conduction mechanism was confirmed to be small polaron conduction.^{11, 15} Defect species are represented according to Kröger–Vink notation and an ideal solution approximation is applied according to the partial molar enthalpy of oxygen in $\text{Sr}_3\text{Fe}_2\text{O}_{7-\delta}$.³⁷ In the localized electron model, mixed valence states of divalent Fe ion, $\text{Fe}_{\text{Fe}}^{\times}$, trivalent Fe ion, $\text{Fe}_{\text{Fe}}^{\cdot}$, and tetravalent Fe ion, $\text{Fe}_{\text{Fe}}^{\times}$, are considered. Oxygen vacancy located in the apical O1 sites connecting the FeO_6 octahedral along the c axis, $V_{\text{O}1}^{\cdot}$, and oxygen vacancy located in equatorial O3 sites, $V_{\text{O}3}^{\cdot}$, are considered as oxygen defect species. The incorporation of oxygen into the O1 sites, and the oxygen vacancy re-distribution between the O1 and O3 sites from the oxygen lattice can be expressed as



The equilibrium constants for reactions (8), K_{OX} , and (9), K_1 , are represented by

$$K_{\text{OX}} = \frac{[\text{O}_{\text{O}1}^{\times}][\text{Fe}_{\text{Fe}}^{\times}]^2}{P(\text{O}_2)^{1/2}[V_{\text{O}1}^{\cdot}][\text{Fe}_{\text{Fe}}^{\cdot}]^2} \frac{\gamma_{[\text{O}_{\text{O}1}^{\times}]} \gamma_{[\text{Fe}_{\text{Fe}}^{\times}]}}{\gamma_{[V_{\text{O}1}^{\cdot}]} \gamma_{[\text{Fe}_{\text{Fe}}^{\cdot}]}} \quad (10)$$

$$K_1 = \frac{[\text{O}_{\text{O}1}^{\times}][V_{\text{O}3}^{\cdot}]}{[V_{\text{O}1}^{\cdot}][\text{O}_{\text{O}3}^{\times}]} \frac{\gamma_{[\text{O}_{\text{O}1}^{\times}]} \gamma_{[V_{\text{O}3}^{\cdot}]}}{\gamma_{[V_{\text{O}1}^{\cdot}]} \gamma_{[\text{O}_{\text{O}3}^{\times}]}} \quad (11)$$

where γ_i is the activity coefficient of component i . Additionally, the disproportionation of charge carrier among $\text{Fe}_{\text{Fe}}^{\cdot}$, $\text{Fe}_{\text{Fe}}^{\times}$ and $\text{Fe}_{\text{Fe}}^{\times}$ occurs

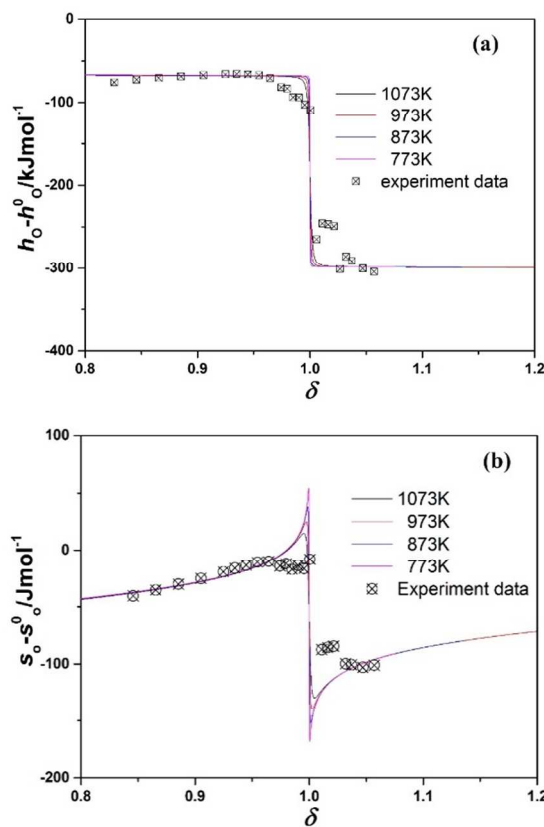


Fig.7 Partial molar enthalpy and entropy of oxygen for $\text{Sr}_3\text{Fe}_2\text{O}_{7-\delta}$. Solid lines are calculated by Eqs. (44) and (45).



For which the equilibrium constant is given by:

$$K_f = \frac{[\text{Fe}_{\text{Fe}}^{\cdot}][\text{Fe}_{\text{Fe}}^{\times}]}{[\text{Fe}_{\text{Fe}}^{\cdot}]^2} \frac{\gamma_{[\text{Fe}_{\text{Fe}}^{\cdot}]} \gamma_{[\text{Fe}_{\text{Fe}}^{\times}]}}{\gamma_{[\text{Fe}_{\text{Fe}}^{\cdot}]}} \quad (13)$$

Gibbs free energy changes in the reactions (8), (9), and (12) can be expressed by

$$\Delta G_{\text{OX}}^{\circ} = -RT \ln K_{\text{OX}} = -RT \ln \frac{[\text{O}_{\text{O}1}^{\times}][\text{Fe}_{\text{Fe}}^{\times}]^2}{P(\text{O}_2)^{1/2}[V_{\text{O}1}^{\cdot}][\text{Fe}_{\text{Fe}}^{\cdot}]^2} - RT \ln \frac{\gamma_{[\text{O}_{\text{O}1}^{\times}]} \gamma_{[\text{Fe}_{\text{Fe}}^{\times}]}}{\gamma_{[V_{\text{O}1}^{\cdot}]} \gamma_{[\text{Fe}_{\text{Fe}}^{\cdot}]}} \quad (14)$$

$$\Delta G_1^{\circ} = -RT \ln K_1 = -RT \ln \frac{[\text{O}_{\text{O}1}^{\times}][V_{\text{O}3}^{\cdot}]}{[V_{\text{O}1}^{\cdot}][\text{O}_{\text{O}3}^{\times}]} - RT \ln \frac{\gamma_{[\text{O}_{\text{O}1}^{\times}]} \gamma_{[V_{\text{O}3}^{\cdot}]}}{\gamma_{[V_{\text{O}1}^{\cdot}]} \gamma_{[\text{O}_{\text{O}3}^{\times}]}} \quad (15)$$

$$\Delta G_f^{\circ} = -RT \ln K_f = -RT \ln \frac{[\text{Fe}_{\text{Fe}}^{\cdot}][\text{Fe}_{\text{Fe}}^{\times}]}{[\text{Fe}_{\text{Fe}}^{\cdot}]^2} - RT \ln \frac{\gamma_{[\text{Fe}_{\text{Fe}}^{\cdot}]} \gamma_{[\text{Fe}_{\text{Fe}}^{\times}]}}{\gamma_{[\text{Fe}_{\text{Fe}}^{\cdot}]}} \quad (16)$$

The standard Gibbs free energy changes for the reactions (8), (9), and (12) can be expressed by $\Delta G_{\text{OX}}^{\circ}$, ΔG_1° , and ΔG_f° . An ideal solution approximation is applied to the reactions (8), (9) and (12), then, activity coefficients in Eqs. (10), (11) and (13) are unity.

The ratios of anion sites to cation sites for $\text{Sr}_3\text{Fe}_2\text{O}_{7-\delta}$ are given by

$$[\text{Sr}_{\text{Sr}}^{\times}] = 3 \quad (17)$$

$$[\text{Fe}_{\text{Fe}}^{\cdot}] + [\text{Fe}_{\text{Fe}}^{\times}] + [\text{Fe}_{\text{Fe}}^{\times}] = 2 \quad (18)$$

$$[V_{\text{O}1}^{\cdot}] + [\text{O}_{\text{O}1}^{\times}] = 1 \quad (19)$$

$$[\text{O}_{\text{O}2}^{\times}] = 2 \quad (20)$$

$$[V_{\text{O}3}^{\cdot}] + [\text{O}_{\text{O}3}^{\times}] = 4 \quad (21)$$

The charge neutrality is given by

$$2[\text{Fe}_{\text{Fe}}^{\text{e}}] + [\text{Fe}_{\text{Fe}}^{\text{h}}] = 2([\text{V}_{\text{O}1}^{\text{v}}] + [\text{V}_{\text{O}3}^{\text{v}}]) \quad (22)$$

The amount of oxygen nonstoichiometry, δ , is given by

$$\delta = [\text{V}_{\text{O}1}^{\text{v}}] + [\text{V}_{\text{O}3}^{\text{v}}] \quad (23)$$

From Eqs. (8)-(23), we obtain the relationship between δ and $P(\text{O}_2)$

$$[\text{V}_{\text{O}1}^{\text{v}}] = \frac{-(4K_1 - K_1\delta + \delta + 1) \pm \sqrt{(4K_1\delta - K_1\delta + \delta + 1)^2 + 4\delta(K_1 - 1)}}{2(K_1 - 1)} \quad (24-1)$$

$$[\text{Fe}_{\text{Fe}}^{\text{e}}] = \frac{-4 \pm \sqrt{16 - 4(4K_f - 1)(4\delta^2 - 8\delta)}}{2(4K_f - 1)} \quad (24-2)$$

$$P(\text{O}_2)^{\frac{1}{2}} = \frac{(1 - [\text{V}_{\text{O}1}^{\text{v}}])(4 - 2\delta - [\text{Fe}_{\text{Fe}}^{\text{e}}])^2}{4[\text{V}_{\text{O}1}^{\text{v}}][\text{Fe}_{\text{Fe}}^{\text{e}}]^2} \exp\left(\frac{\Delta G_{\text{OX}}^{\circ}}{RT}\right) \quad (24-3)$$

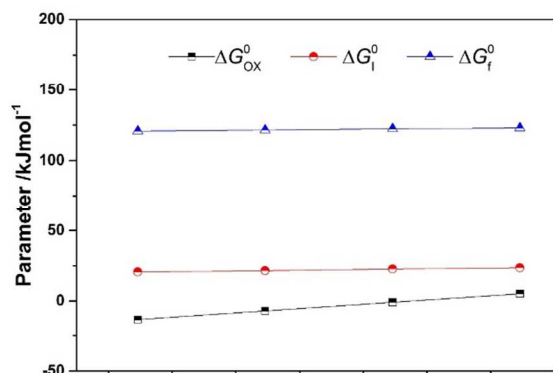


Fig. 8 Fitting parameters ($\Delta G_{\text{OX}}^{\circ}$, $\Delta G_{\text{I}}^{\circ}$, and $\Delta G_{\text{f}}^{\circ}$) for the defect equilibrium model with temperature.

The relationship between δ and $P(\text{O}_2)$ can be represented by Eq. (24) with the fitting parameters, $\Delta G_{\text{OX}}^{\circ}$, $\Delta G_{\text{I}}^{\circ}$, and $\Delta G_{\text{f}}^{\circ}$. The solid curves in Fig. 4 show the fitting results which are in good agreements with the experimental data for all temperatures. The fitting parameters, $\Delta G_{\text{OX}}^{\circ}$, $\Delta G_{\text{I}}^{\circ}$, and $\Delta G_{\text{f}}^{\circ}$, are given for the localized electron model in Fig. 8. The standard enthalpy and entropy changes for the oxygen incorporation reaction, $\Delta H_{\text{OX}}^{\circ}$ and $\Delta S_{\text{OX}}^{\circ}$, the oxygen vacancy redistribution between the O1 and O3 sites from the oxygen lattice, $\Delta H_{\text{I}}^{\circ}$ and $\Delta S_{\text{I}}^{\circ}$, and the disproportionation of iron-ion reaction, $\Delta H_{\text{f}}^{\circ}$ and $\Delta S_{\text{f}}^{\circ}$, were obtained from the slope and intercept of the Van't Hoff plot for $\Delta G_{\text{OX}}^{\circ}$, $\Delta G_{\text{I}}^{\circ}$, and $\Delta G_{\text{f}}^{\circ}$, respectively, according to:

$$\frac{\Delta G_{\text{I}}^{\circ}}{RT} = \ln K_{\text{I}} = \frac{\Delta H_{\text{I}}^{\circ}}{RT} - \frac{\Delta S_{\text{I}}^{\circ}}{R} \quad (25)$$

Table 1

The values of the standard enthalpy (kJmol^{-1}) and entropy changes

$\Delta H_{\text{OX}}^{\circ}$	$\Delta S_{\text{OX}}^{\circ}$	$\Delta H_{\text{I}}^{\circ}$	$\Delta S_{\text{I}}^{\circ}$	$\Delta H_{\text{f}}^{\circ}$	$\Delta S_{\text{f}}^{\circ}$
-60.481	-61.177	12.864	-10.052	115.109	-7.4158

($\text{Jmol}^{-1}\text{K}^{-1}$) for reactions (8), (9) and (12) are summarized

The values of the standard enthalpy and entropy changes for reactions (8), (9) and (12) are summarized in Table 1. Fig. 9(a) shows that the point defect concentration of $\text{Fe}_{\text{Fe}}^{\text{e}}$ and $\text{Fe}_{\text{Fe}}^{\text{h}}$ calculated by the defect equilibrium model fitting as functions of $P(\text{O}_2)$ and temperatures, presenting a proportional dependence as following,

$$[\text{Fe}_{\text{Fe}}^{\text{h}}] \propto P(\text{O}_2)^{0.242} \quad (26)$$

$$[\text{Fe}_{\text{Fe}}^{\text{e}}] \propto P(\text{O}_2)^{-0.248} \quad (27)$$

According to the conductor mechanism of $\text{Sr}_3\text{Fe}_2\text{O}_{7-\delta}$, the p- and n-type concentrations ($[\text{Fe}_{\text{Fe}}^{\text{h}}] - [\text{Fe}_{\text{Fe}}^{\text{e}}]$) of electronic charge carriers are proportional to $P(\text{O}_2)^{1/4}$ and $P(\text{O}_2)^{-1/4}$, respectively.^{11, 14-16} In addition, under reducing conditions, the n-type concentration of $[\text{Fe}_{\text{Fe}}^{\text{e}}]$ shows good agreements with $P(\text{O}_2)$ dependence and the minor deviations originate from non-ideal behavior. But under oxidizing conditions where the oxygen-ion conductivity starts to significantly change relative to oxygen nonstoichiometry, the p-type concentration of $[\text{Fe}_{\text{Fe}}^{\text{h}}]$ can't follow the linear relationship.

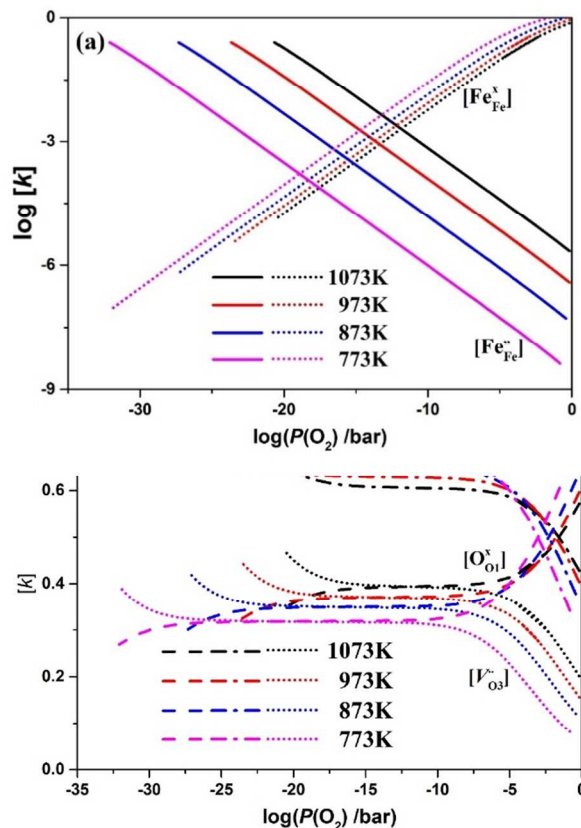


Fig. 9 Calculated point-defect concentrations of electron-hole ($\text{Fe}_{\text{Fe}}^{\text{e}} - \text{Fe}_{\text{Fe}}^{\text{h}}$) (a) and oxygen species (b) depend on the $P(\text{O}_2)$ and temperatures. $[k]$ is the equilibrium point-defect concentration related to one formula unit.

Fig. 9(b) shows the concentrations of oxygen species depend on the $P(\text{O}_2)$ and temperatures of 773-1073 K. By the defect equilibrium model fitting, under low oxygen vacancy concentration, the most oxygen vacancies are firstly located at O1-sites and a small amount of vacancies are located at O3-sites, indicating that a smaller oxygen-ion conductivity can be obtained due to a lower oxygen-ion transport with the pathways of $\text{O}3 \rightarrow \text{O}1 \rightarrow \text{O}3$ jumps along the octahedral edges. With the increasing oxygen vacancy concentration, the rapid increases of oxygen vacancies at O1-sites and at O3-sites were observed, however, the increased speeds of oxygen vacancies at O1-sites at low temperatures are much faster than those at higher temperatures, thus results in the abnormal changes of the oxygen concentration have been observed under high oxygen vacancy concentration that the concentration of $[\text{V}_{\text{O}1}^{\text{v}}]$ gradually decreases with increasing temperature from 773 K to 1173 K, suggesting that

the oxygen vacancy redistribution between the O1 and O3 sites from the oxygen lattice happens. To better explain the oxygen vacancy redistribution between the O1 and O3 sites at intermediate temperatures, it is well known that the Ruddlesden–Popper oxide $\text{Sr}_3\text{Fe}_2\text{O}_{7-\delta}$ possesses several different oxygen-ion transport pathways compared typical perovskite $\text{SrFeO}_{3-\delta}$, where the energy barrier for oxygen-ion transport pathways of $\text{O3} \rightarrow \text{O1} \rightarrow \text{O3}$ jumps (0.9–1.4 eV) is much smaller than that of directly $\text{O3} \rightarrow \text{O3}$ jumps (1.5–2.2 eV).^{14, 16} Therefore, oxygen vacancy redistribution from the O1 sites to O3 sites is apparent to maintain adequate oxygen-ion transport pathways of $\text{O3} \rightarrow \text{O1} \rightarrow \text{O3}$ jumps with low energy barrier, suggesting that $\text{Sr}_3\text{Fe}_2\text{O}_{7-\delta}$ is a nice self-adjusting for adequate oxygen-ion conductivity.

3.3 Statistical thermodynamic calculation for $\text{Sr}_3\text{Fe}_2\text{O}_{7-\delta}$

Mizusaki *et al.* clearly presented the theoretical relationship between the defect equilibrium model and thermodynamic quantities and the calculated results by the statistical thermodynamic calculation agree with the thermodynamic quantities determined by the δ - T - $P(\text{O}_2)$ relationship.^{34,36,38-39} In order to elucidate the relationship between the defect structure and thermodynamic quantities in $\text{Sr}_3\text{Fe}_2\text{O}_{7-\delta}$, the statistical thermodynamic calculation with localized electrons is derived from the Gibbs free energy of the system and defect equilibrium model.

The Gibbs free energy of the system, G , is expressed by

$$G = G^\circ + \sum_i x_i \mu_i^\circ + \sum_i x_i RT \ln \gamma_i x_i \quad (28)$$

where x and μ represent the molar fraction and the chemical potential, respectively. Here we assume that μ° and γ quasi-chemical species are independent of δ . The oxygen chemical potential in $\text{Sr}_3\text{Fe}_2\text{O}_{7-\delta}$ is the differentiation of G with the number of moles of oxygen, $7-\delta$. Then, μ_{O} can be calculated by

$$\begin{aligned} \mu_{\text{O}} &= \frac{\partial G}{\partial (7-\delta)} = -\frac{\partial G}{\partial \delta} = \\ &= -\left(\sum_i \frac{\partial x_i}{\partial \delta} \mu_i^\circ + \sum_i \frac{\partial x_i}{\partial \delta} RT \ln \gamma_i + \frac{\partial}{\partial x} \sum_i x_i RT \ln x_i \right) \end{aligned} \quad (29)$$

The configurational entropy of $\text{Sr}_3\text{Fe}_2\text{O}_{7-\delta}$ with localized electrons, $S(\text{conf})$, can be calculated by

$$\begin{aligned} S(\text{conf}) &= k \left[\ln \left(\frac{(3N_A)!}{([\text{Sr}_{\text{Sr}}]N_A)!} \right) + \ln \left(\frac{(2N_A)!}{([\text{Fe}_{\text{Fe}}]N_A)!([\text{Fe}_{\text{Fe}}^\times]N_A)!([\text{Fe}_{\text{Fe}}^\circ]N_A)!} \right) + \right. \\ &\left. \ln \left(\frac{(7N_A)!}{([\text{O}_{\text{O1}}^\times]N_A)!([\text{V}_{\text{O1}}^\circ]N_A)!([\text{O}_{\text{O2}}^\times]N_A)!([\text{O}_{\text{O3}}^\times]N_A)!([\text{V}_{\text{O3}}^\circ]N_A)!} \right) \right] \end{aligned} \quad (30)$$

where k is the Boltzmann constant. The partial molar entropy due to the configurational entropy, $s_{\text{O}}(\text{conf})$, is obtained by the differentiation of $S(\text{conf})$ with respect to δ . From the Stirling's approximation and the relation of $R = k N_A$, $s_{\text{O}}(\text{conf})$ can be calculated by

$$s_{\text{O}}(\text{conf}) = -\frac{\partial S(\text{conf})}{\partial \delta} = R \frac{\partial}{\partial \delta} \left(\sum_i x_i \ln x_i \right) \quad (31)$$

Eqs. (18), (22) and (24-2) and Eqs. (19), (21), (23) and (24-1) are differentiations by δ , respectively. The variable quantities of $\frac{\partial [\text{Fe}_{\text{Fe}}^\times]}{\partial \delta}$, $\frac{\partial [\text{Fe}_{\text{Fe}}^\circ]}{\partial \delta}$, $\frac{\partial [\text{Fe}_{\text{Fe}}^\times]}{\partial \delta}$, $\frac{\partial [\text{V}_{\text{O1}}^\circ]}{\partial \delta}$, $\frac{\partial [\text{O}_{\text{O1}}^\times]}{\partial \delta}$, $\frac{\partial [\text{V}_{\text{O3}}^\circ]}{\partial \delta}$ and $\frac{\partial [\text{O}_{\text{O3}}^\times]}{\partial \delta}$ can be calculated.

$$\frac{\partial [\text{Fe}_{\text{Fe}}^\times]}{\partial \delta} = \frac{2[\text{Fe}_{\text{Fe}}][\text{Fe}_{\text{Fe}}^\times] + 4[\text{Fe}_{\text{Fe}}^\times][\text{Fe}_{\text{Fe}}^\circ]}{[\text{Fe}_{\text{Fe}}][\text{Fe}_{\text{Fe}}^\times] + [\text{Fe}_{\text{Fe}}][\text{Fe}_{\text{Fe}}^\circ] + 4[\text{Fe}_{\text{Fe}}^\times][\text{Fe}_{\text{Fe}}^\circ]} \quad (32)$$

$$\frac{\partial [\text{Fe}_{\text{Fe}}^\circ]}{\partial \delta} = \frac{2[\text{Fe}_{\text{Fe}}][\text{Fe}_{\text{Fe}}^\circ] - 4[\text{Fe}_{\text{Fe}}^\times][\text{Fe}_{\text{Fe}}^\circ]}{[\text{Fe}_{\text{Fe}}][\text{Fe}_{\text{Fe}}^\times] + [\text{Fe}_{\text{Fe}}][\text{Fe}_{\text{Fe}}^\circ] + 4[\text{Fe}_{\text{Fe}}^\times][\text{Fe}_{\text{Fe}}^\circ]} \quad (33)$$

$$\frac{\partial [\text{Fe}_{\text{Fe}}^\times]}{\partial \delta} = \frac{-4[\text{Fe}_{\text{Fe}}][\text{Fe}_{\text{Fe}}^\times] - 2[\text{Fe}_{\text{Fe}}^\times][\text{Fe}_{\text{Fe}}^\circ]}{[\text{Fe}_{\text{Fe}}][\text{Fe}_{\text{Fe}}^\times] + [\text{Fe}_{\text{Fe}}][\text{Fe}_{\text{Fe}}^\circ] + 4[\text{Fe}_{\text{Fe}}^\times][\text{Fe}_{\text{Fe}}^\circ]} \quad (34)$$

$$\frac{\partial [\text{V}_{\text{O1}}^\circ]}{\partial \delta} = \frac{4[\text{V}_{\text{O1}}^\circ](1 - [\text{V}_{\text{O1}}^\circ])}{-5[\text{V}_{\text{O1}}^\circ]^2 + 2\delta[\text{V}_{\text{O1}}^\circ] + 4\delta - \delta^2} \quad (35)$$

$$\frac{\partial [\text{V}_{\text{O3}}^\circ]}{\partial \delta} = 1 - \frac{\partial [\text{V}_{\text{O1}}^\circ]}{\partial \delta} \quad (36)$$

$$\frac{\partial [\text{O}_{\text{O1}}^\times]}{\partial \delta} = -\frac{\partial [\text{V}_{\text{O1}}^\circ]}{\partial \delta} \quad (37)$$

$$\frac{\partial [\text{O}_{\text{O3}}^\times]}{\partial \delta} = \frac{\partial [\text{V}_{\text{O1}}^\circ]}{\partial \delta} - 1 \quad (38)$$

The standard Gibbs free energy changes ($\Delta G_{\text{OX}}^\circ$, $\Delta G_{\text{I}}^\circ$ and $\Delta G_{\text{f}}^\circ$) for the reactions of Eqs. (8), (9) and (12) are expressed

$$\Delta G_{\text{OX}}^\circ = \mu^\circ(\text{O}_{\text{O1}}^\times) + 2\mu^\circ(\text{Fe}_{\text{Fe}}^\times) - \frac{1}{2}\mu^\circ(\text{O}_2(\text{gas})) - \mu^\circ(\text{V}_{\text{O1}}^\circ) - 2\mu^\circ(\text{Fe}_{\text{Fe}}^\circ) \quad (39)$$

$$\Delta G_{\text{I}}^\circ = \mu^\circ(\text{V}_{\text{O3}}^\circ) + \mu^\circ(\text{O}_{\text{O1}}^\times) - \mu^\circ(\text{V}_{\text{O1}}^\circ) - \mu^\circ(\text{O}_{\text{O3}}^\times) \quad (40)$$

$$\Delta G_{\text{f}}^\circ = \mu^\circ(\text{Fe}_{\text{Fe}}^\times) + \mu^\circ(\text{Fe}_{\text{Fe}}^\circ) - 2\mu^\circ(\text{Fe}_{\text{Fe}}^\circ) \quad (41)$$

where $\mu^\circ(\text{O}_2(\text{gas}))$ is the chemical potential of 1 bar oxygen gas, which is related to μ_{O}° by

$$\mu^\circ(\text{O}_2(\text{gas})) = 2\mu_{\text{O}}^\circ \quad (42)$$

The relationship between the statistical thermodynamic model and defect equilibrium model is shown in the following part. The partial molar quantities, μ_{O} - μ_{O}° , h_{O} - h_{O}° and s_{O} - s_{O}° can be simplified to

$$\mu_{\text{O}} - \mu_{\text{O}}^\circ = \Delta G_{\text{OX}}^\circ - \left(1 - \frac{\partial [\text{V}_{\text{O1}}^\circ]}{\partial \delta} \right) \Delta G_{\text{I}}^\circ - \frac{\partial [\text{Fe}_{\text{Fe}}^\times]}{\partial \delta} \Delta G_{\text{f}}^\circ - T s_{\text{O}}(\text{conf}) \quad (43)$$

$$h_{\text{O}} - h_{\text{O}}^\circ = \Delta H_{\text{OX}}^\circ - \left(1 - \frac{\partial [\text{V}_{\text{O1}}^\circ]}{\partial \delta} \right) \Delta H_{\text{I}}^\circ - \frac{\partial [\text{Fe}_{\text{Fe}}^\times]}{\partial \delta} \Delta H_{\text{f}}^\circ \quad (44)$$

$$s_{\text{O}} - s_{\text{O}}^\circ = \frac{\Delta S_{\text{OX}}^\circ}{4} - \left(1 - \frac{\partial [\text{V}_{\text{O1}}^\circ]}{\partial \delta} \right) \frac{\Delta S_{\text{I}}^\circ}{4} - \frac{\partial [\text{Fe}_{\text{Fe}}^\times]}{\partial \delta} \frac{\Delta S_{\text{f}}^\circ}{4} + s_{\text{O}}(\text{conf}) \quad (45)$$

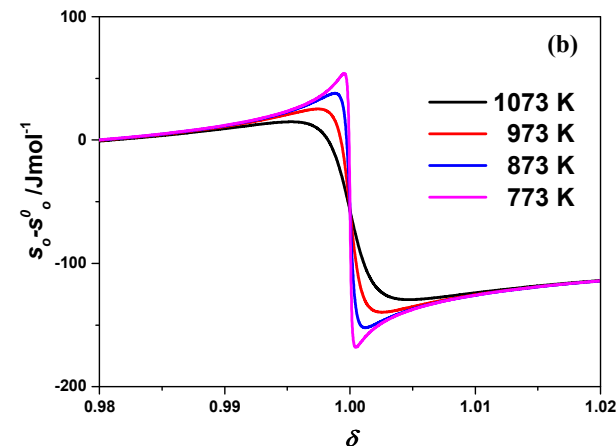
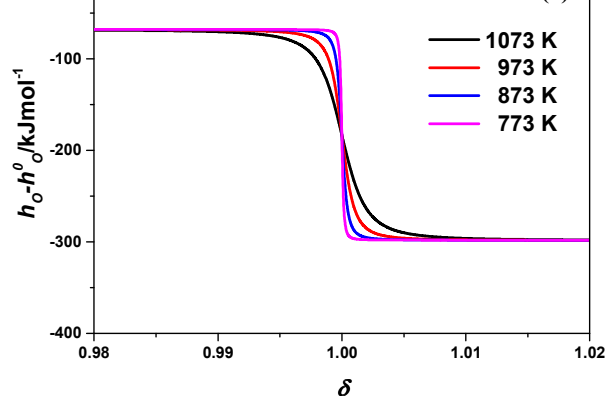


Fig.11 Temperature dependence of $h_{\text{O}} - h_{\text{O}}^\circ$ (a) and $s_{\text{O}} - s_{\text{O}}^\circ$ (b) calculated from the statistical thermodynamic calculation in the oxygen nonstoichiometry range 0.98–1.02.

Eqs. (43)–(45) give the relationships of the partial molar quantities and the parameters determined for the defect equilibrium model in $\text{Sr}_3\text{Fe}_2\text{O}_{7-\delta}$. Fig. 5 and Fig. 7 also show the partial molar quantities of

$\text{Sr}_3\text{Fe}_2\text{O}_{7-\delta}$ calculated from the statistical thermodynamic calculation, and the behaviors of $h_{\text{O}} - h_{\text{O}}^{\circ}$ and $s_{\text{O}} - s_{\text{O}}^{\circ}$ seem to deviate from those using the Gibbs–Helmholtz equation around $\delta=1$. Fig. 10 shows the thermodynamic quantities of $\text{Sr}_3\text{Fe}_2\text{O}_{7-\delta}$ at 773–1073 K calculated from the statistical thermodynamic calculation in the oxygen nonstoichiometry range 0.98–1.02, indicating the changes of $h_{\text{O}} - h_{\text{O}}^{\circ}$ and $s_{\text{O}} - s_{\text{O}}^{\circ}$ around $\delta=1$ become more drastic with different temperatures and the assumption for the calculation by the Gibbs–Helmholtz equation is not satisfied. To more clearly illustrate the phenomenon, Fig. 11 reflects the tendency of $\frac{\partial[\text{Fe}_{\text{Fe}}^{\bullet}]}{\partial\delta}$ and $\frac{\partial[V_{\text{O}1}]}{\partial\delta}$ depend on the narrow range of δ . It can be easily understood that the behaviors of calculated curves of $h_{\text{O}} - h_{\text{O}}^{\circ}$ and $s_{\text{O}} - s_{\text{O}}^{\circ}$ result from the tendency of $\frac{\partial[\text{Fe}_{\text{Fe}}^{\bullet}]}{\partial\delta}$ with the temperature dependence of K_{f} . Therefore, the relationship between the thermodynamic quantities, the defect equilibrium model, and the defect equilibrium of $\text{Sr}_3\text{Fe}_2\text{O}_{7-\delta}$ is more clearly shown by using the statistical thermodynamic calculation and defect equilibrium model.

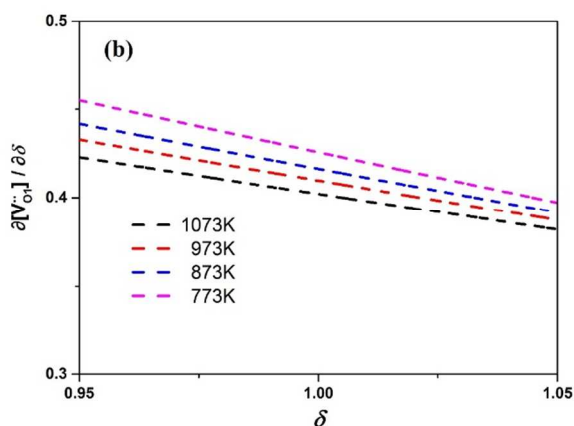
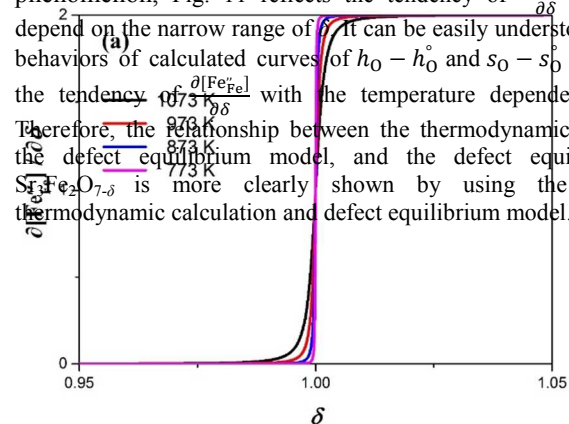


Fig. 11 Tendency of $\frac{\partial[\text{Fe}_{\text{Fe}}^{\bullet}]}{\partial\delta}$ (a) and $\frac{\partial[V_{\text{O}1}]}{\partial\delta}$ (b) depend on the narrow range of δ according to the statistical thermodynamic calculation.

4. Conclusions

Oxygen nonstoichiometry of the Ruddlesden–Popper oxide $\text{Sr}_3\text{Fe}_2\text{O}_{7-\delta}$ at intermediate temperatures (773–1073K) and the $P(\text{O}_2)$ range between the decomposition $P(\text{O}_2)$ and 1 bar was measured by the coulometric titration and the high temperature gravimetry, where

the $P(\text{O}_2)$ dependencies of the oxygen nonstoichiometry exhibited typical plateaus at $\delta \sim 1.0$, where the average oxidation state of iron is 3+. Oxygen nonstoichiometry of $\text{Sr}_3\text{Fe}_2\text{O}_{7-\delta}$ can be explained by the defect equilibrium model with localized electrons with an ideal solution approximation. By the defect equilibrium model, the point defect concentrations of $\text{Fe}_{\text{Fe}}^{\bullet}$ and $\text{Fe}_{\text{Fe}}^{\times}$ are proportional to $P(\text{O}_2)^{-0.248}$ and $P(\text{O}_2)^{0.242}$, and the oxygen vacancy redistribution between the O1 and O3 sites from the oxygen lattice was estimated. The obtained thermodynamic quantities of the oxygen chemical potential, $\mu_{\text{O}} - \mu_{\text{O}}^{\circ}$, the partial molar enthalpy of oxygen, $h_{\text{O}} - h_{\text{O}}^{\circ}$, and partial molar entropy of oxygen, $s_{\text{O}} - s_{\text{O}}^{\circ}$, are in good agreements with ones from the statistical thermodynamic calculation. The relationship between the thermodynamic quantities, the defect equilibrium model, and the defect equilibrium of $\text{Sr}_3\text{Fe}_2\text{O}_{7-\delta}$ is more clearly shown by using the statistical thermodynamic models and defect equilibrium model.

Acknowledgement

The authors wish to thank Japan Society for the Promotion of Science (JSPS) for financial support through a Post-doctoral Fellowship for Foreign Researchers.

References

- Institute of Multidisciplinary Research for Advanced Materials, Tohoku University, 2-1-1 Katahira Aoba-ku, Sendai 980–8577, Japan. E-mail: ling@mail.tagen.tohoku.ac.jp. Fax: +81 (0)22 217 5343; Tel: +81 (0)22 217 5340
- Graduate School of Environmental Studies, Tohoku University, 6-6-01 Aramaki Aoba-ku, Sendai 980–8579, Japan
- M. Yashima, M. Enoki, T. Wakita, R. Ali, Y. Matsushita, F. Izumi and T. Ishihara, *J. Am. Chem. Soc.*, 2008, **130**, 2762.
- A. Tarancón, S. J. Skinner, R. J. Chater, F. Hernandez-Ramírez and J. A. Kilner, *J. Mater. Chem.*, 2007, **17**, 3175.
- G. Kim, S. Wang, A. J. Jacobson, L. Reimus, P. Brodersen and C. A. Mims, *J. Mater. Chem.*, 2007, **17**, 2500.
- E. Boehm, J. M. Bassat, P. Dordor, F. Mauvy, J. C. Grenier and P. Stevens, *Solid State Ionics*, 2005, **176**, 2717;
- M. Burriel, G. Garcia, J. Santiso, J. A. Kilner, R. J. Chater and S. J. Skinner, *J. Mater. Chem.*, 2008, **18**, 416.
- A. Chang, S. J. Skinner and J. A. Kilner, *Solid State Ionics*, 2006, **177**, 2009.
- F. Prado and A. Manthiram, *J. Solid State Chem.*, 2001, **158**, 307.
- Y.A. Shilova, M.V. Patrakeev, E.B. Mitberg, I.A. Leonidov and V.L. Kozhevnikov, *J. Solid State Chem.*, 2002, **168**, 275.
- L. Mogni, F. Prado, and A. Caneiro, *Chem. Mater.*, 2006, **18**, 4163
- L. Mogni, J. Fouletier, F. Prado and A. Caneiro, *J. Solid State Chem.*, 2005, **178**, 2715.
- M.V. Patrakeev, I.A. Leonidov, V.L. Kozhevnikov and V.V. Kharton, *Solid State Sci.*, 2004, **6**, 907.
- I. Kagomiya, K. Jimbo, K. Kakimoto, M. Nakayama and O. Masson, *Phys. Chem. Chem. Phys.*, 2014, **16**, 10875
- F. Prado, L. Mogni, G.J. Cuello and A. Caneiro, *Solid State Ionics*, 2007, **178**, 77.
- A.A. Markov, M.V. Patrakeev, V.V. Kharton, Y.V. Pivak, I.A. Leonidov and V.L. Kozhevnikov, *Chem. Mater.*, 2007, **19**, 3980.
- L.V. Mogni, F.D. Prado, G.J. Cuello and A. Caneiro, *Chem. Mater.*, 2009, **21**, 2614.
- V.V. Kharton, M.V. Patrakeev, E.V. Tsipis, M. Avdeev, E.N. Naumovich, P.V. Anikina and J.C. Waerenborgh, *Solid State Ionics*, 2010, **181**, 1052.

- 17 S. Diethelm, A. Closset, J. Van Herle and K. Nisancioglu, *Electrochemistry*, 2000, **68**, 444.
- 18 L. Wang, R. Merkle, J. Maier, T. Acartürk and U. Starke, *Appl. Phys. Lett.*, 2009, **94**, 071908
- 19 F. Prado, T. Armstrong, A. Caneiro and A. Manthiram, *J. Electrochem. Soc.*, 2001, **148**, J7-J14.
- 20 S. B. Adler, *J. Am. Ceram. Soc.*, 2001, **84**, 2117-2119.
- 21 A. Atkinson and T. Ramos, *Solid State Ionics*, 2000, **129**, 259-269.
- 22 Bruker AXS, User's Manual (2008) Bruker AXS, Karlsruhe, Germany.
- 23 D. Pelloquin, J. Hadermann, M. Giot, V. Caignaert, C. Michel, M. Hervieu and B. Raveau, *Chem. Mater.*, 2004, **16**, 1715.
- 24 M. Matvejeff, M. Lehtimäki, A. Hirasa, Y.H. Huang, H. Yamauchi and M. Karppinen, *Chem. Mater.*, 2005, **17**, 2775
- 25 M. Lehtimäki, A. Hirasa, M. Matvejeff, H. Yamauchi and M. Karppinen *J. Solid State Chem.*, 2007, **180**, 3247
- 26 M. Lehtimäki, H. Yamauchi and M. Karppinen, *J. Solid State Chem.*, 2013, **204**, 95.
- 27 J. Mizusaki, H. Tagawa, K. Naraya and T. Sasamoto, *Solid State Ionics*, 1991, **49**, 111
- 28 J. Mizusaki, N. Mori, H. Takai, Y. Yonemura, H. Minamiue, H. Tagawa, M. Dokiya, H. Inaba, K. Naraya, T. Sasamoto and T. Hashimoto, *Solid State Ionics*, 2000, **129**, 163.
- 29 M. Kuhn, Y. Fukuda, S. Hashimoto, K. Sato, K. Yashiro and J. Mizusaki, *J. Electrochem. Soc.*, 2013, **160** (1), F34
- 30 T. Nakamura, K. Yashiro, K. Sato and J. Mizusaki, *Solid State Ionics*, 2009, **180**, 368.
- 31 M. Arnold, H.H. Wang and A. Feldhoff, *J. Membr. Sci.*, 2007, **293**(1-2), 44.
- 32 M. Arnold, T.M. Gesing, J. Martynczuk and A. Feldhoff, *Chem. Mater.*, 2008, **20**(18), 5851.
- 33 K.H. Ryu and S.M. Haile, *Solid State Ionics*, 1999, **125**, 355.
- 34 J. Mizusaki, M. Yoshihiro, S. Yamauchi and K. Fueki, *J. Solid State Chem.*, 1987, **67**, 1
- 35 M. Kuhn, S. Hashimoto, K. Sato, K. Yashiro and J. Mizusaki, *J. Solid State Chem.*, 2013, 197, 38.
- 36 T. Nakamura, K. Yashiro, K. Sato and J. Mizusaki, *J. Solid State Chem.*, 2009, 182, 1121.
- 37 F.A. Kröger, *The Chemistry of Imperfect Crystals Vol. 2* 2nd revised edition, North Holland Publishing Company, Netherlands, 1974 Chap. 7 and 9.
- 38 J. Mizusaki, M. Yoshihiro, S. Yamauchi and K. Fueki, *J. Solid State Chem.*, 1985, **58**, 257.
- 39 T. Nakamura, K. Yashiro, K. Sato and J. Mizusaki, *Solid State Ionics*, 2009, **180**, 1406.